Birefringence-based eye fixation monitor with no moving parts

B. I. Gramatikov
O. H. Y. Zalloum
Y. K. Wu
Johns Hopkins University School of Medicine
Wilmer Ophthalmological Institute
The Krieger Children's Eye Center
Baltimore, Maryland 21287-9028
E-mail: bgramat@jhmi.edu

D. G. Hunter
Harvard Medical School
Children's Hospital Boston
Department of Ophthalmology
Boston, Massachusetts

D. L. Guyton
Johns Hopkins University School of Medicine
Wilmer Ophthalmological Institute
The Krieger Children's Eye Center
Baltimore, Maryland 21287-9028

Abstract. For the purpose of vision screening, we develop an eye fixation monitor that detects the fovea by its unique radial orientation of birefringent Henle fibers. Polarized near-infrared light is reflected from the foveal area in a bow-tie pattern of polarization states, similar to the Haidinger brush phenomenon. In contrast to previous devices that used scanning systems, this instrument uses no moving parts. It rather utilizes four spots of linearly polarized light—two aligned with the "bright" arms and two aligned with the "dark" arms—of the bow-tie pattern surrounding the fovea. The light reflected from the fundus is imaged onto a quadrant photodetector, whereby the circular polarization component of the polarization state of each reflected patch of light is measured. The signals from the four photodetectors are amplified, digitized, and analyzed. A normalized differential signal is computed to detect central fixation. The algorithm is tested on a computer model, and the apparatus is tested on human subjects. This work demonstrates the feasibility of a fixation monitor with no moving parts.
[DOI: 10.1117/1.2209003]

Keywords: polarized light; birefringence; eye fixation; fovea.

Paper 05138RR received Jun. 13, 2005; revised manuscript received Mar. 1, 2006; accepted for publication Mar. 3, 2006; published online May 31, 2006.

1 Introduction

In the late 1980s, human foveal birefringence was measured *in vivo* with Mueller-matrix ellipsometry.[1] In the early 1990s, the birefringence of the retinal nerve fibers was utilized by Dreher, Reiter, and Weinreb,[2] to measure the thickness of the nerve fiber layer. On hearing this presentation in 1991, Guyton reasoned that the birefringence of the nerve fibers surrounding the human fovea (Henle fibers) might be used to detect their strict radial geometry. Such a technique could be used to monitor foveal fixation and thus to detect proper alignment of the two eyes in infants and young children. After prolonged experimentation, he reported implementation of this technique in 2000.[3]

Using the optics of the eye in an autoconjugate arrangement, our first instruments employed a circular scanning system.[3–5] When the eye fixated and focused on the target, the light reflected from the retina was automatically focused by the eye back to the source, where it was deflected by a beamsplitter and measured.

Polarized near-infrared light is reflected from the foveal area in a bow-tie pattern of polarization states; the pattern is similar to the faint pattern observed surrounding the point of fixation when a subject views a clear background through a polarized filter (the Haidinger brush phenomenon[6]). With our previous instruments, the foveal area was probed with a circular scan of frequency f. When the eye fixated on a point at the center of the circular scan, the double-pass polarization state of the light changed at twice the frequency of the scan ($2f$). With paracentral fixation, the change in the polarization state was only at the frequency of the scan (f).

We subsequently developed and reported a binocular portable eye fixation monitor for early detection of strabismus in children.[4,7] In this personal computer (PC)-supported device, a point source of polarized near-infrared light was imaged onto the retina and scanned in a 3-deg-diam circle. Reflections were analyzed by differential polarization detection, employing a polarizing beamsplitter for each eye, with measurement trains obtained several times each second. The detected signal was predominantly $2f$ during central fixation, and f with paracentral fixation. The screener detected misalignment of the eyes of subjects of all ages, including young children. This method, however, required a rapidly spinning motor, which added noise and vibration and which was generally of limited life. To avoid these problems, we have explored the feasibility of a no-moving-parts version of the instrument using a four-quadrant photodetector. This eye fixation sensor has allowed precise detection of central fixation in five subjects.

2 Methods

2.1 *Instrument Design*

The new instrument utilizes four spots of vertically linearly polarized light—two aligned with the "bright" arms and two aligned with the "dark" arms—of the bow-tie pattern of polarization states of the light reflected from the fovea (Fig. 1).

Address all correspondence to Boris Gramatikov, Wilmer Eye Institute, Johns Hopkins University, 600 N. Wolfe St. - Wilmer, Rm. 233, Baltimore, Maryland 21287. Tel: 410 614 6017; Fax: 410 955 0809; E-mail address: bgramat@jhmi.edu

1083-3668/2006/11(3)/034025/11/$22.00 © 2006 SPIE

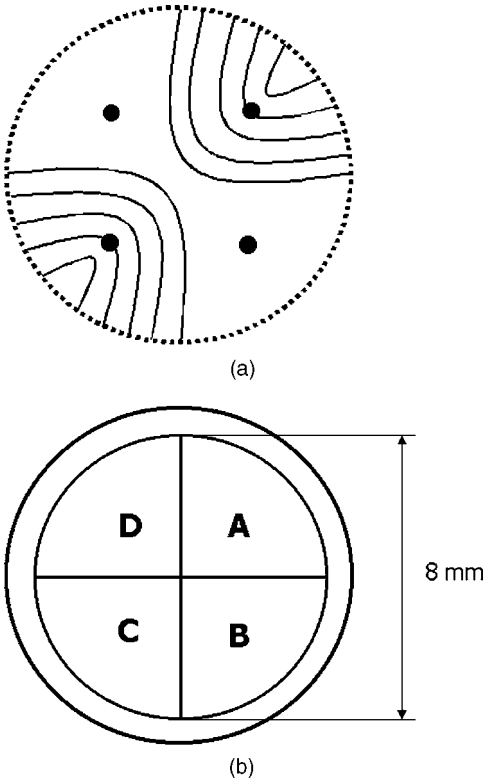

Fig. 1 Principle of the birefringence-based eye fixation monitor with no moving parts: each quadrant photosensor of the four-quadrant photodetector receives reflected light from the respective patch of light within the arms of the bow-tie pattern. (a) Bow-tie pattern of polarization states surrounding the fovea, and the four spots of light aligned with the arms of the pattern. (b) Four-quadrant photodetector (Centrovision QD50-0) oriented to receive reflected light from the four illuminated patches.

The four spots are produced from a single 780-nm, 100-mW laser diode using a multifaceted prism (Fig. 2). The laser output is modulated by a square wave ($f=140$ Hz) to improve the signal-to-noise ratio. A near-infrared wavelength was selected to minimize reflex pupillary constriction and thus loss of power,[8] and to maximize spectral reflectance compared with visible wavelengths.[9,10] Safe light levels were used at all times.[11]

The light reflected from the fundus travels through a quarter-wave plate and a polarizer, and is then imaged onto a quadrant photodetector of 8 mm diam, whereby the circular polarization component of the polarization state of each reflected patch of light is measured (Fig. 3). In the Stokes vector representation of the polarization state $S=\{S_0,S_1,S_2,S_3\}$, S_3 represents the differential measurement of the circular polarization component (right-handed circular polarization minus left-handed circular polarization).[12,13] In our device, we measure the circular polarization component by first rotating the polarization states on the Poincaré sphere 90 deg by means of the quarter-wave plate, and then measuring the linear polarization along the S_1 axis using a polarizer in front of the detector. Rather than obtaining the differential measurement along the S_1 axis, which would require a polarizing beamsplitter and two detectors, we measure using only one polarizer and one detector for each of our four patches of light. As explained later, we then mathematically obtain a spatial differential measurement by subtracting the signals from the patches in the dark arms of the bow-tie pattern from the signals from the patches in the bright arms. The double-pass corneal birefringence can interfere with this measurement, and this is analyzed later.

The fixation target is a small, translucent smiley face that is rear illuminated with a whitelight LED. This fixation target is located in the center of a square, whose corners are the four

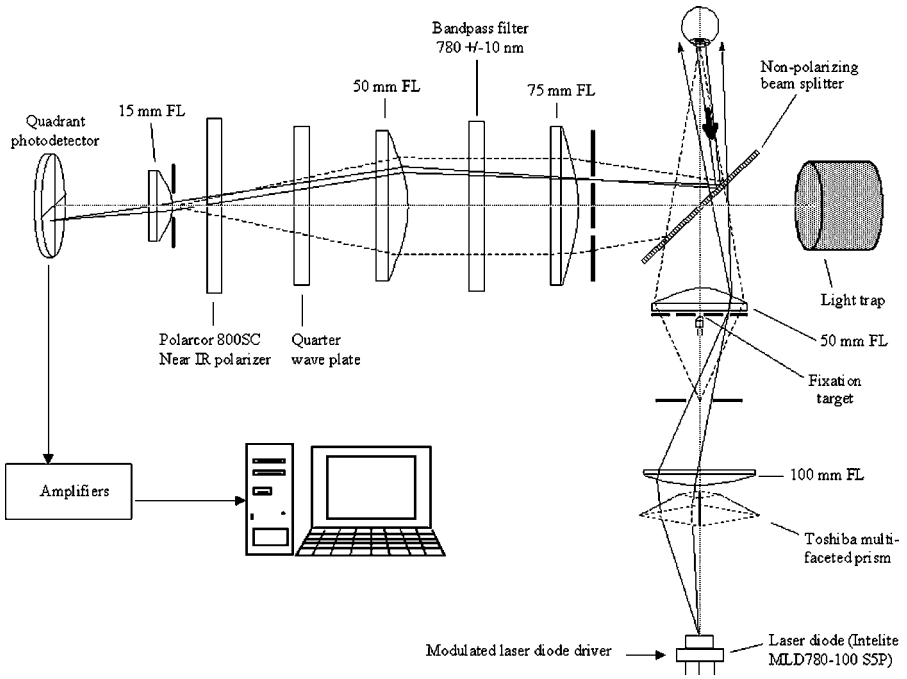

Fig. 2 Instrument design, showing the illumination and detection light paths for one of the four spots of light, not to scale.

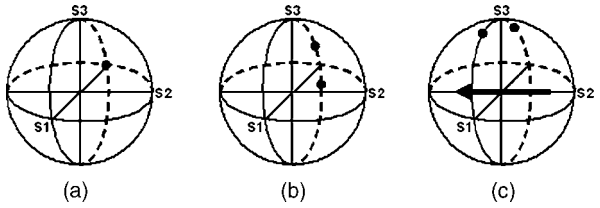

Fig. 3 Poincaré sphere representations of the basic polarization states used. (a) Input polarization is linear and vertically oriented, represented as $S_1=-1$. (b) The upper dot represents the polarization state of the patches of light reflected from both bright arms, and the lower dot represents the polarization state of the patches of light reflected from both dark arms. Note that it is the circular polarization component of these states that is maximally different (separated primarily in the S_3 direction). (c) A quarter-wave plate has rotated all the polarization states 90 deg about its fast axis (represented by the eigenvector in the equatorial plane), so that the differences in the circular polarization component can now be conveniently measured along the S_1 axis.

faintly red light spots seen by the test subject. The four signals from the four photodetectors are amplified, filtered, and transmitted to a PC for analog-to-digital conversion (using a 200-ms epoch length) and further digital analysis (Fig. 4). Signal processing includes mainly bandpass digital filtering at the modulation frequency of 140 Hz, synchronous signal averaging of 28 waveforms, and background subtraction, for each of the four channels. The number of waveforms analyzed corresponds to the number of times the measurement cycle of 7.14 ms (140 Hz) is contained in the 200-ms epoch. Software was written by us in C language (CVI, National Instruments) and includes a graphical user interface, data acquisition, signal analysis, and routines for signal and trend visualization, plotting, and signal statistics.

The illuminated area at the surface of the eye is approximately 30×30 mm to allow for movement of the head during fixation in anticipation of future vision screening applications.[3–5] Background noise is caused by lid and facial reflections and by internal instrument reflections. The amplitude of the noise is approximated by obtaining a measurement with the eyes closed. This background signal is collected prior to each set of fixation measurements, stored separately for each channel, and subtracted from the fixation readings.

2.2 *Computer Model of the Four-Quadrant Fixation Monitor*

To optimize the detection algorithm, we developed in MATLAB a mathematical model of the fixation monitor signals [Figs. 5(a) and 5(b)]. The model represents an idealized 2-D spatial intensity profile of the polarization-altered light reflected from the fundus, after passing through the quarter-wave plate and polarizer overlying the detector. The signal in each detector quadrant is calculated by integrating the light intensity point-wise across the area captured by each particular detector quadrant. Since the optical design uses four patches of light on the retina, the model uses a mask, thus sensing only light reflected by the four patches directly illuminated by the laser. All other parts of the retina are assumed not to contribute to the signal. Each patch of light always falls in the middle of a quadrant, but can be reflected from any part of the fovea or parafovea, depending on where the eye is

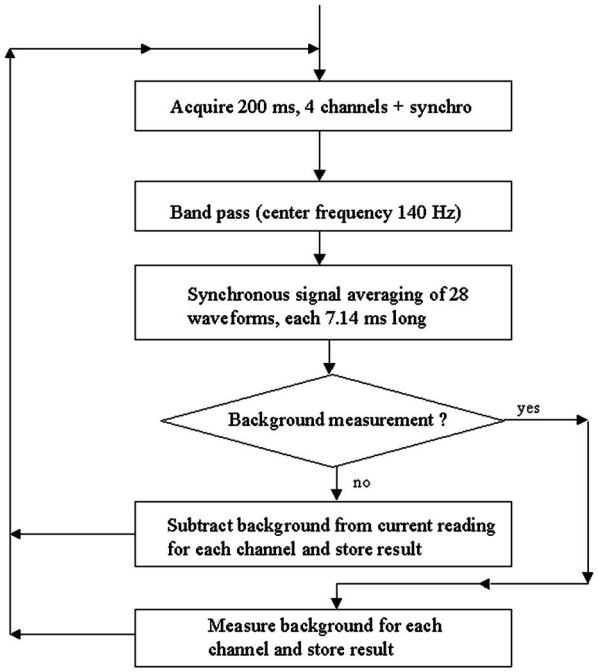

Fig. 4 Digital signal processing algorithm (simplified).

"fixing." For simplicity, this model takes into account some blurring on the retina due to imperfect imaging on the single pass into the eye. It does not take into account additional blurring that may occur on the return path back out of the eye. The model rather behaves as if a four-quadrant detector were placed immediately above the retina on the return path.

The bow-tie distribution of light intensities, upon passing through the polarizer overlying the quadrant detector, is shown in Fig. 5(a). This assumes strict radial orientation of the Henle fibers, which is indeed the case within the central 5 deg centered on the fovea.[14] It was modeled with a $\cos^2(\theta)$ function, where θ is the azimuth with respect to the fast axis of the Henle fiber birefringence. To achieve attenuation in the regions away from the center, this cosine function was modulated with an exponential radial function of the shape shown in Fig. 6, derived from previous measurements in our laboratory.[15] The overall bow-tie light intensity function used (FB) was

$$FB=[\cos(\theta)]^2\left[\prod_{i=1}^{2}\exp\left(-\frac{r}{\tau_i}\right)\right]\left\{\prod_{i=3}^{5}\left[1-\exp\left(-\frac{r}{\tau_i}\right)\right]\right\}, \tag{1}$$

where θ is the azimuth relative to the fast axis of the Henle fiber birefringence $\theta=a\tan(y_b/x_b)$, and $r=(x_b^2+y_b^2)^{1/2}$ is the distance from the origin of the bow-tie distribution in millimeters, on the same scale as the bow-tie image on the surface of the photodetector. The exponents that give the closest match to the profile shown in Fig. 6 are as follows: $\tau_1=3.7$, $\tau_2=50.0$, $\tau_3=0.6$, $\tau_4=5.0$, and $\tau_5=0.8$. The model uses millimeters in the detector plane (1.96 mm/deg of visual angle).

With central fixation, the center of the detector and the center of the foveal bow-tie pattern should coincide. The signals received by quadrants A and C are equal to each other, as

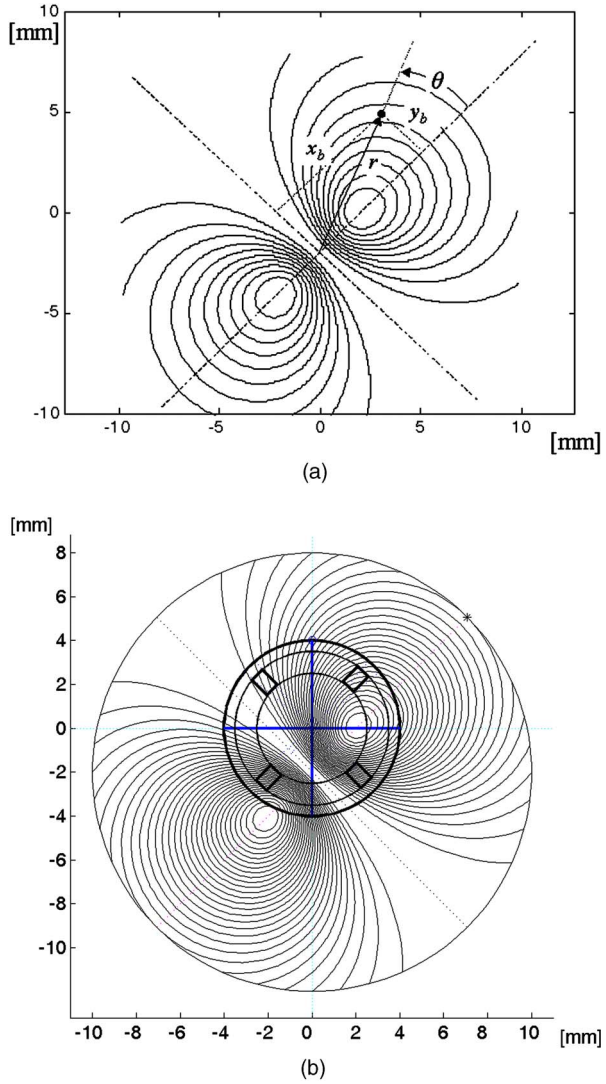

Fig. 5 The mathematical model. (a) An idealized 2-D spatial intensity profile of the light reflected from the fundus, after passing through the quarter-wave plate and polarizer (1 deg of visual angle=1.96 mm at the photodetector). (b) An idealized 2-D spatial intensity profile of the light reflected from the fundus, after passing through the quarter-wave plate and polarizer, and falling on the plane of the quadrant photodetector. The signal in each detector quadrant is calculated by integrating the intensity signal point-wise for the illuminated (square) area corresponding to each patch of light. In this particular case, the eye is looking 1 deg upward from the center, and therefore the center of the fovea is shifted by 2 mm downward with respect to the center of the photodetector. There is no horizontal displacement.

are the signals received by quadrants B and D. When the eye looks away from the center (paracentral fixation), the two centers no longer coincide, as shown in Fig. 5(b), where the eye is looking 1-deg upwards from the center. The signals from quadrants A and C are no longer equal, nor are the signals received by quadrants B and D. Depending on the direction of gaze, different portions of the bow-tie intensity pattern are projected onto the four quadrants of the photodetector.

In the model, the center of the bow-tie intensity pattern can be positioned at any point in the plane of the photodetector. For each position of the bow-tie center (point x,y), the model yields a set of signals $[A,B,C,D]$ corresponding to the signals received from the four detector segments of the four-quadrant photodetector.

2.3 *Central Fixation Equation*

If A,B,C, and D are the signals from the four-quadrant photodetector, counted in the clockwise direction (Fig. 1), with A and C corresponding to the areas yielding higher intensities than areas B and D, then a differential signal (diff) is obtained by subtracting the signals of the anticipated lower intensity quadrants from those of the higher intensity quadrants:

$$\text{diff} = (A + C) - (B + D).$$

In this formula, all four signals obtained from human subjects are used after subtraction of background. Normalization is applied to eliminate the influence of individual differences in fundus reflectance, and to adjust for intensity variation due to corneal birefringence. The normalized differential signal (ND) is:

$$\text{ND} = \frac{(A + C) - (B + D)}{A + B + C + D}. \quad (2)$$

The signal ND is highest with central fixation, where A and C are at a maximum positive and B and D are at a maximum negative, thus detecting central fixation when the signal exceeds an empirically determined threshold.

To create a spatial representation, ND was plotted in the X and Y directions away from the center of the bow-tie pattern in 0.25-deg (visual angle) increments, with interpolation (Figs. 7 and 8). The output of the mathematical model of the fixation monitor is plotted in Fig. 7, showing ND at each X and Y position of the bow-tie light intensity pattern with respect to the detector. The ND was calculated from the set of the quadrant signals A,B,C, and D, according to Eq. (2). The same type of plot, obtained from signals A,B,C, and D using Eq. (2) for central and paracentral fixation from data from a representative subject (1 in the table), is shown in Fig. 8.

2.4 *Human Subjects*

Five adults (three male and two female), aged 23 to 60, were tested. The study was approved by the Institutional Review Board for all measurements described here, and written consent was obtained properly in writing from each subject. The subjects had no history of eye disease and had corrected visual acuity of 20/20 or better in the tested eye.

2.5 *Collection and Analysis of Human Central Fixation Data*

To characterize the signals obtained from human eyes, a 2-D eccentric viewing scale, graduated in degrees of visual angle, was reflected into the light path of the fixation detector via a 1-mm-thick lantern slide cover slip serving as a beamsplitter. The scale was centered on the central fixation point, allowing the subject to fixate on any intersection of the grid at known coordinates relative to the center of the four laser spots. Each measurement was background-corrected, and the average of five measurements was used for each point. Points with large variance within the measurement set were discarded and spa-

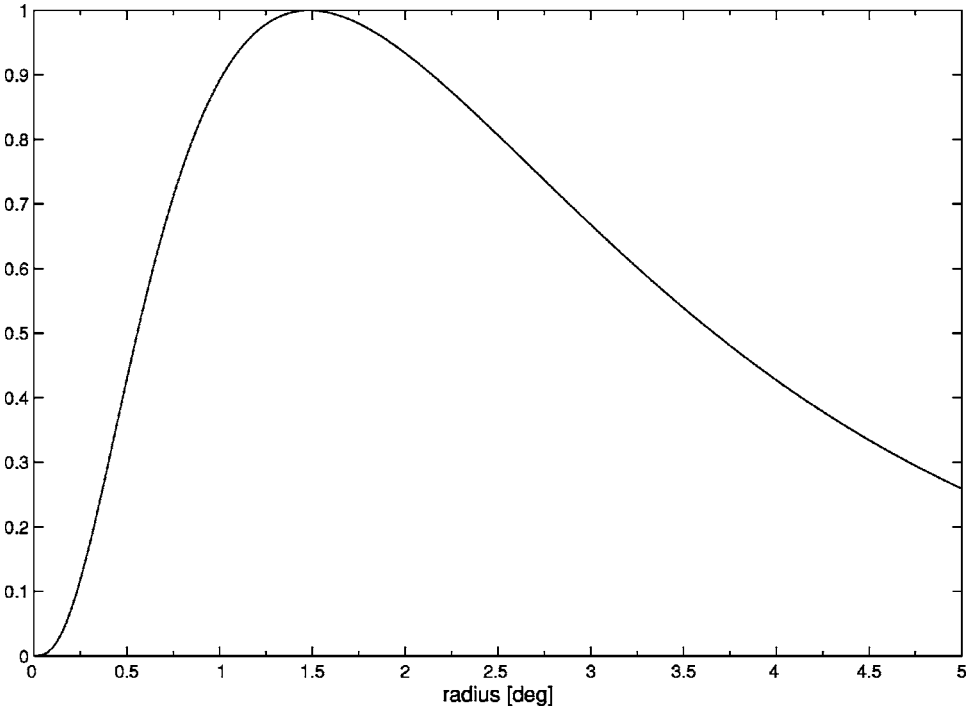

Fig. 6 Change of the strength of the Henle fiber birefringence signal as a function of the distance from the foveal center as measured in the plane of the photodetector (1 deg of visual angle=1.96 mm at the photodetector).

tially interpolated during plotting. For each node (1 deg $\times$1 deg grid intersection), the average $\boldsymbol{a}_i=[A_iB_iC_iD_i]$ was recorded, thus obtaining data from the $11\times11=121$ main grid nodes. In addition, data from the central region within a radius of 2 deg were collected using half-degree grid spacings. The ND was calculated using Eq. (2), and plotted as an *X-Y* 2-D distribution.

2.6 *Mathematical Model for Assessing the Influence of Corneal Birefringence on the Orientation of the Bow Tie*

The intensity bow tie shown in Figs. 1(a), 5(a), and 5(b) is oriented at 45 deg. In reality, the bow-tie orientation depends on the polarization properties of the incident beam, as well as on the birefringence of the cornea. For a vertically polarized incident beam, as in our system, an orientation of 45 deg occurs when the corneal retardance is equal to zero. To study the influence of the retardance and azimuth of the corneal birefringence on the orientation of the bow tie, we used a modified version of a computer model previously developed in our laboratory.[5] Briefly, this model describes mathematically retinal birefringence scanning (RBS) in a double-pass system using Stokes vector analysis and Mueller matrix multiplication. The cornea was modeled as a linear retarder, whereas the foveal area was modeled as a radially symmetric birefringent medium. The model has been shown to accurately predict the frequency and phase of RBS signals obtained with our eye fixation monitor[3,4] during central and paracentral fixation. The method is based on analysis of polarization changes induced by the retina and cornea, and by reflection from the fundus:

$$\begin{aligned}\mathbf{S}_{\text{out}} &= \mathbf{M}\times\mathbf{S}_{\text{in}}\\ \mathbf{M} &= \mathbf{M}(\theta_c,\delta_c)\times\mathbf{M}(\theta_r,\delta_r)\times\mathbf{M}_{\text{reff}}\\ &\quad\times\mathbf{M}(-\theta_r,\delta_r)\times\mathbf{M}(-\theta_c,\delta_c),\end{aligned}\tag{3}$$

where $\mathbf{S}$ is the four-element Stokes vector, and $\mathbf{M}$ is the 4 $\times$4 Mueller matrix, whose values are functions of the azimuth θ and the retardance δ of the corresponding retarder.[12] Since we use vertically polarized light, the incident Stokes vector is $\mathbf{S}_{\text{in}}=\{1,-1,0,0\}$ (unit intensity beam used). In the previous equation, the subscript r stands for *retinal*, while the subscript c stands for *corneal*. Thus, the polarization state of light is altered when light passes [Eq. (3), left to right] through the cornea, then through the retina (the birefringent radially symmetric Henle fibers surrounding the fovea), and is then reflected by the deeper layers of the retina, and returns through the retina and cornea. The typical values for θ_r, δ_r, θ_c, and δ_c are given in our laboratory's previous work.[4] During a scan, the values of θ_r and δ_r at each moment depend on the position of the scanned spot of light on the nerve fiber layer surrounding the fovea. The azimuth θ_r of the retinal retardance depends on the orientation of the fibers at the point being scanned, while the retinal retardance δ_r depends on the distance from the foveal center [we used the radial function from Eq. (1) for this purpose]. The ocular fundus at our wavelength (780 nm) exhibits a high degree of polarization preservation[2] and can be modeled with a good approximation as a reflective surface. The $\mathbf{M}_{\text{refl}}$ is

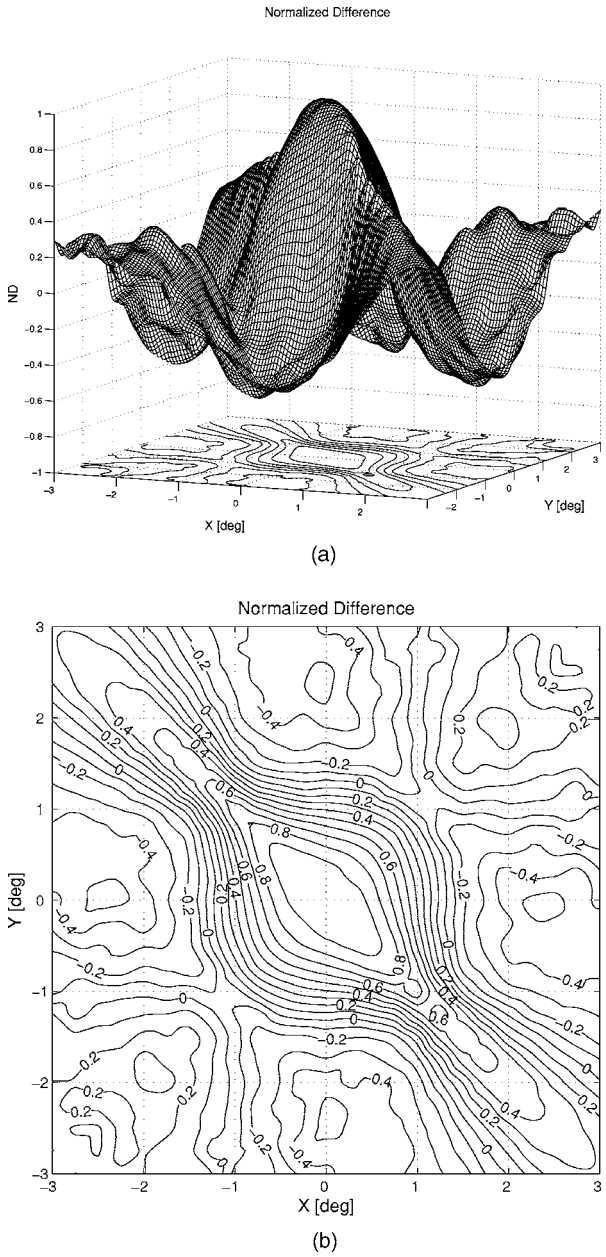

Fig. 7 Result of the model for the normalized difference ND as a function of the distance between foveal origin and the center of the four-quadrant photodetector. The distance is in degrees of visual angle.

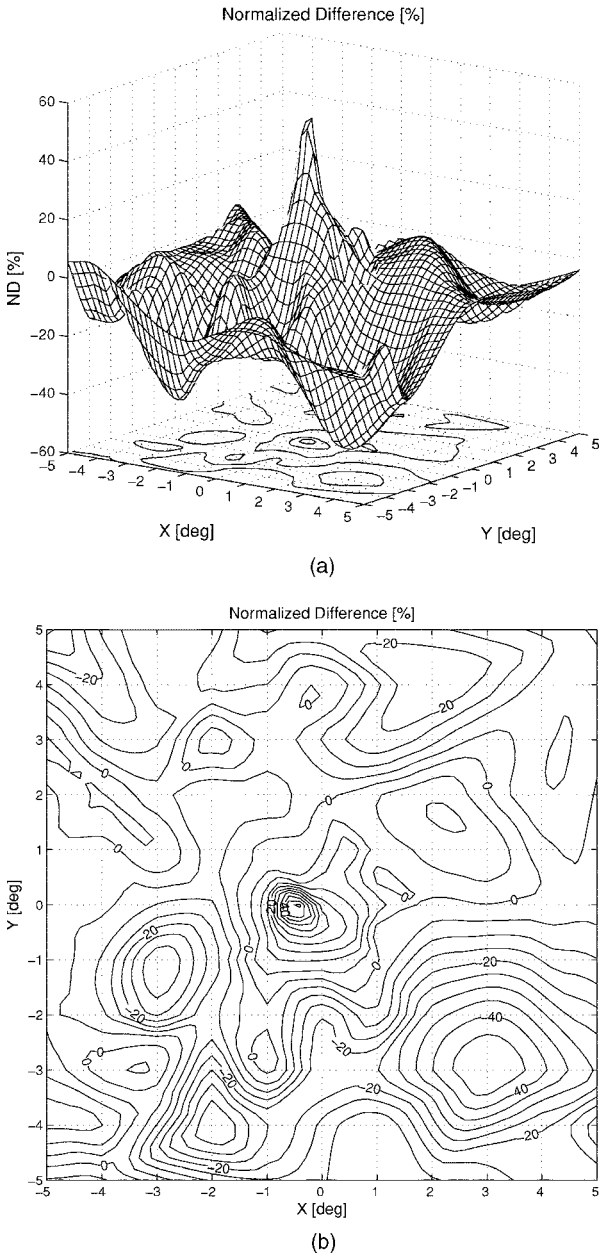

Fig. 8 The normalized difference ND as a function of the direction of gaze of a human eye. The measurements were done using a 2-D eccentric viewing scale. The contour lines in (b) are at 5% intervals.

$$\mathbf{M}_{\text{refl}} = \begin{bmatrix} 1 & 0 & 0 & 0 \\ 0 & 1 & 0 & 0 \\ 0 & 0 & -1 & 0 \\ 0 & 0 & 0 & -1 \end{bmatrix},$$

which simply changes the sign of Stokes vector elements S_2 and S_3. The 180-deg phase change at reflection thus reverses the sign of the azimuth and the handedness of the reflected polarized light. In the Mueller matrices for the retina and cornea for the return pass, (θ) has been replaced by $(-\theta)$. The model provides all four elements of the output $\mathbf{S}_{\text{out}}$, thus enabling comparison among the utilities of the four Stokes components for retinal birefringence scanning. All calculations in this model are performed in MATLAB.

To obtain the phase of the scanning signal and the orientation of the Haidinger-type bow tie, in our RBS model we "spun" the scanning beam in a circle around the center of the fovea, and calculated S_3. This provided the amplitude of the signal that would have been recorded by a single photodetector for each point on the scanning 360-deg circle (instead of using a four-quadrant photodetector). The position of the first maximum of the signal was assumed to coincide with the orientation of the bow-tie axis. This corresponds to the bow-tie maximum at 45 deg (CCW from the three o'clock horizontal direction) in the illustrative examples in Figs. 1(a),

5(a), and 5(b). Indeed, a 360-deg scan obtained from the model with corneal retardance set to zero produces a sine wave with its first maximum at 45 deg, indicating that Figs. 1(a), 5(a), and 5(b) assume zero corneal retardance. Further, we wrote a shell program that calculates and plots the bow-tie angle as a function of corneal azimuth (CA) and corneal retardance (CR) for numerous locations on the CA-CR plane.

As a source of corneal birefringence measurements on a large number of human subjects, we used the data published by Knighton and Huang[16] and kindly provided to us in numerical form by the authors. This study determined the polarization properties of central cornea at perpendicular incidence in a normal human population (73 normal subjects), assuming that the cornea behaves as a linear retarder. We refer to this data as the Bascom Palmer Eye Institute (BPEI) data. A similar dataset can be obtained from another study published in the same year,[17] where healthy and glaucomatous eyes were studied.

2.7 *Measuring the Corneal Birefringence of the Test Subjects in this Study*

For our five test subjects, we wished to compare the predicted output from our model to our actual measurements. This could be done only if we knew their individual corneal birefringences. To measure the corneal birefringence in terms of retardance and azimuth of each subject, we utilized the commercial GDx-VCC instrument (Carl Zeiss Meditec), available in the authors' institution. The GDx, mainly used in glaucoma diagnosis, measures the retinal nerve fiber layer (RNFL) thickness, which is proportional to the measured retardation when polarized light passes through the birefringent RNFL. The variable corneal compensator (VCC) version of the instrument allows individual compensation of corneal birefringence by first measuring the corneal retardance and azimuth, and then adjusting the VCC accordingly, which consists of two linear retarders in rotating mounts.[18] Compensation occurs when the fast axis of the variable retarder is parallel to the slow axis of the measured corneal birefringence, and when the retardance of the VCC matches the measured corneal retardance. We upgraded the device to software version 5.5.0, which gives access to the measured corneal birefringence.

2.8 *Finding an Optimal Compensator for Corneal Birefringence*

With the goal of minimizing the error due to different bow-tie orientation with different corneal birefringence, we developed an algorithm and related software for calculating a fixed compensator retarder that, for the available BPEI dataset, would statistically maximize the number of eyes with bow-tie orientation within a certain range around 45 deg. In the RBS model, we inserted a retarder $\mathbf{M}(\theta_{comp}\delta_{comp})$, operating on both the incoming and the return path:

$$\mathbf{M} = \mathbf{M}(\theta_{\text{comp}}, \delta_{\text{comp}}) \times \mathbf{M}(\theta_c, \delta_c) \times \mathbf{M}(\theta_r, \delta_r) \times \mathbf{M}_{\text{refl}} \times \mathbf{M}(-\theta_r, \delta_r) \times \mathbf{M}(-\theta_c, \delta_c) \times \mathbf{M}(-\theta_{\text{comp}}, \delta_{\text{comp}}).$$

Optimization was achieved by varying the compensator properties on a grid covering 0 to 100-nm retardance, and 0 to 50 deg fast axis orientation (measured nasally downward). For each node on this grid, the bow-tie orientation was calculated for all eyes from the BPEI dataset, and a goodness criterion as the portion of the eyes (RE+LE) with bow-tie axis within ±5 deg of the "normal" 45 deg (corneal retardance 0) was calculated and plotted. The grid node with the highest goodness number was chosen to be the best corneal compensator.

3 Results

3.1 *Central Fixation in the Main Model*

The output of the mathematical model of the fixation monitor is plotted in Fig. 7, showing ND at each X and Y position of the bow-tie light intensity pattern with respect to the detector. The ND was calculated from the set of the quadrant signals A, B, C, and D, according to Eq. (2). A definite maximum can be seen at central fixation (0,0). For a desired level of precision, a corresponding threshold can be set, above which central fixation can be assumed based on the value of the ND function alone. In the model shown, a threshold of ND=0.8 permits detection of central fixation with an accuracy better than 0.8 deg.

3.2 *Central Fixation in the Tested Human Subjects*

3.2.1 *Measured data*

In the five human eyes tested, ND during central fixation ranged from 0.1968 to 0.3645 [mean=0.2711, standard deviation (SD)=0.0713]. The data from all five subjects are presented in Table 1. The composite signal-to-noise ratio (measured as the sum of all four channels compared to the composite background noise) ranged from 0.07 to 0.14 (mean=0.104, SD=0.032). During fixation on any paracentral location on the grid, ND was always <0.07. ND was negative in many paracentral locations. For central and paracentral fixation, the data from a representative subject (1 from the table) are shown in Fig. 8. The ND distribution exhibits a distinct peak of about 0.5 attributable to central fixation, although shifted by ca. −0.5 deg in the X direction, possibly due to a less-than-perfect centration. Note that on the contour plot [Fig. 8(b)], the value at eye position (0,0) is about 0.23, which is quite close to the ND=0.1968 obtained in a separate measurement for the same subject (1).

3.2.2 *Predicted data*

The corneal birefringence data measured from the five test subjects with the GDx instrument (as described in Sec. 2.7) are presented in columns 4 and 5 of Table 1 (right eye). The corneal axis (azimuth) is measured in degrees, with nasally downward considered positive. These values, for each subject separately, were inserted into the RBS model, which calculated the bow-tie orientation according to Sec. 2.6, and are given in column 6 of the table. It can be seen that for these subjects, the change of the bow-tie tilt is between −1 and −5 deg. Similarly, we found for the left eye changes between 0 and 3 deg, in the mirror image direction. Using the bow-tie orientation from column 6, we ran the four-quadrant model to calculate the normalized distance ND_{calc} in column 7. These calculations show that for our test subjects, corneal birefringence only minimally influences the ND as a measure of central fixation.

Table 1 Measured and predicted values for the test subjects in this study. The second and third columns represent measurements with our device. The next two columns are corneal measurements taken with the GDx-VCC. The last two columns are predicted values for the bow-tie orientation and for the corresponding calculated ND under ideal conditions, respectively.

			Measured corneal birefringence (with the GDx-VCC)			
Subject	Measured normalized difference $ND_{measured}$	Signal-to-noise ratio	Retardance [nm]	Axis [deg] (nasally down)	Calculated bow-tie orientation [deg] (RBS model)	Calculated normalized difference ND_{calc} (4Q model)
1	0.1968	0.0715	19	24	44	1.00
2	0.3038	0.0710	17	7	44	1.00
3	0.2024	0.1075	28	41	44	1.00
4	0.3645	0.1420	30	14	42	0.99
5	0.2878	0.1279	40	27	40	0.98
Average	0.2711	0.1040	26.80	22.60	42.8	0.99
STD	0.0713	0.0323	9.26	13.01	1.8	0.01

3.3 *Assessing the Influence of Corneal Birefringence on the Orientation of the Bow Tie Using the Bascom Palmer Eye Institute Data*

To assess the role of corneal birefringence on a larger dataset, we applied our RBS model (described in Sec. 2.6) to the BPEI data. During simulated central fixation, we scanned along an annulus of 3 deg around the fovea with a vertically polarized incident beam. The model was run for each of the 143 eyes in the dataset (71 right eyes and 72 left eyes of 73 subjects). Since our RBS model expected the corneal fast axis, the following calculations were performed:

$$CA_{FA} = CA_{SA} + 90 \text{ deg (right eye)}$$

$$CA_{FA} = -CA_{SA} + 90 \text{ deg (left eye)},$$

where CA_{SA} is a negative value of the corneal slow axis, measured nasally downward for each eye, as in the original dataset. The thus-calculated fast axis CA_{FA} was used along with the corneal retardance CR in the computer model 2.6. For each eye, the position of the first maximum of the computed scan signal was identified as angle β, corresponding to the axis of the bow tie. A 360-deg scan obtained with the RBS model, with corneal retardance equal to zero, yields a sine wave with its first maximum at β=45 deg, consistent with a 45-deg orientation of the bow tie, as indicated in Figs. 1(a) and 5(a). Figures 9(a) and 9(b) show the distribution of the orientation angle β of the first maximum of the bow tie relative to three o'clock, depending on corneal retardance and azimuth, for the right and left eyes, respectively. The BPEI data were superimposed on a full-grid plot of β(CA,CR), where CA is the slow axis, to stay compatible with previous publications. Clearly, for the majority of eyes, the orientation angle β is in the range 30 to 50 deg, but there are certainly "outliers." The same distribution is shown as histograms on Figs. 10(a) and 10(b), for the right and left eye, respectively. It can be seen that corneal birefringence tends to increase the bow-tie orientation angle in left eyes, and to decrease it in right eyes (which is what we also observed in our five subjects). There are 5 out of 71 (7%) right eyes (RE) with orientation angle less than 10 deg, and 9 out of 72 (12.5%) left eyes (LE) with orientation angle less than −40 deg. In fact, the left-most LE case crosses into the next quadrant and can be considered part of the main distribution, in the 80 to 90 deg segment. Our calculations with the four-quadrant model showed that at orientations deviating from 45 deg by up to ±20 deg, the normalized difference still displays a positive maximum at central fixation, but loses up to about 25% of its value. Central fixation in such cases is still detectable, at the cost of a reduced threshold. However, the previously noted outliers are missed by this device.

3.4 *Finding an Optimal Corneal Compensator*

To reduce statistically the influence of the corneal birefringence, we propose the use of a fixed corneal compensator with a fast axis in the quadrant nasally downward for each eye. Applying the algorithm from Sec. 2.8, we obtained Fig. 11, showing the portion of the good eyes with brush orientation within ±5 deg of 45 deg. There is a relatively broad CR-CA region, for which 74% of all (RE+LE) eyes would fall in the good category, with several spots giving 76% coverage. Our algorithm measured a maximum at CR=45 nm, and CA=25 deg (fast axis, nasally downward), which (just as the other spots) happens to be relatively close to the fixed corneal compensator of the earlier GDx-FCC (60 nm/15 deg).[18] With the suggested compensator, the full-

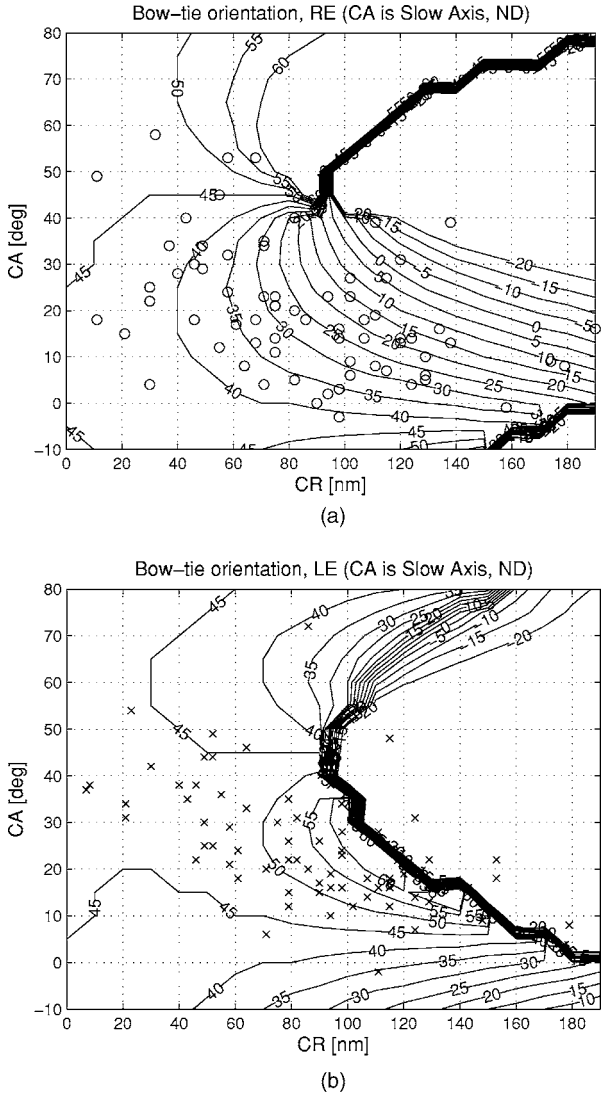

Fig. 9 Bow-tie orientation as a function of corneal retardance and corneal azimuth, with the BPEI data blended in: (a) right eye (71 eyes) and (b) left eye (72 eyes).

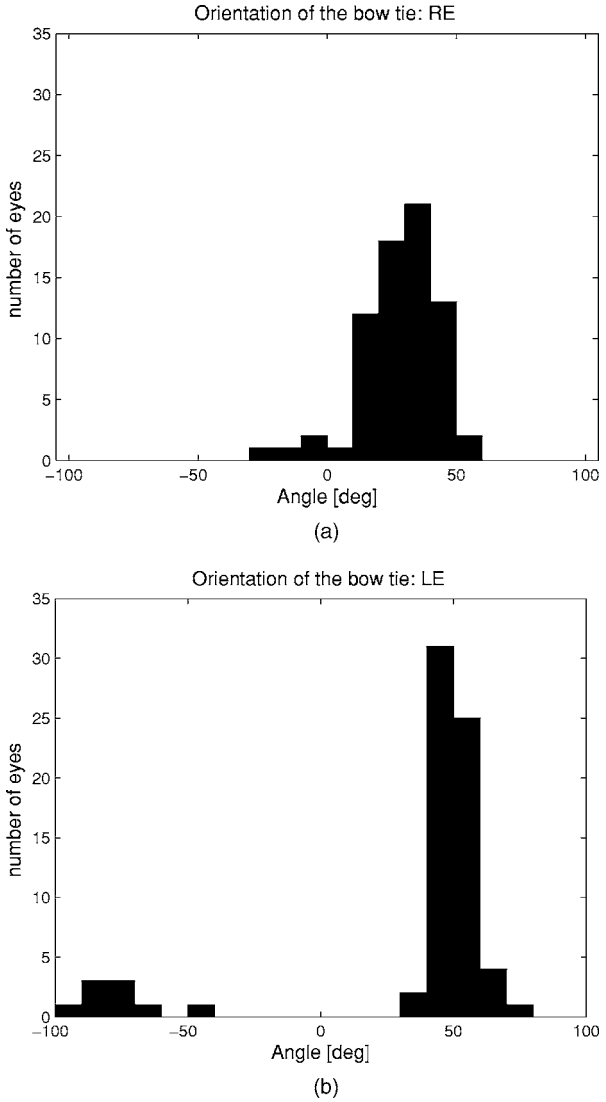

Fig. 10 Distribution of the bow-tie orientation angle from Fig. 9 (BPEI data): (a) Right eye (71 eyes) and (b) left eye (72 eyes).

grid plot of the bow-tie orientation $\beta(\mathrm{CA},\mathrm{CR})$ was calculated and is plotted in Fig. 12, and the distribution histograms are shown in Fig. 13. Within ±5 deg of 45 deg, we now have 49 of 71 (69.01%) RE, 61 of 72 (84.72%) LE, and 110 of 143 (76.92%) for both eyes. A liberal ±22-deg tolerance around 45 deg gives 69 of 71 (97.18%) RE, 72 of 72 (100.00%) LE, and 141 of 143 (98.60%) for both eyes. These results are a significant improvement, compared to the results calculated without a corneal compensator (Figs. 9 and 10). The same algorithm should allow individual optimization for each eye, should a different compensator with fast axis orientation and/or different compensator retardance be allowed for each eye.

4 Discussion

Our laboratory has previously demonstrated how a polarized light scan of the birefringent foveal area can be used to detect fixation by the fovea of the eye. The present study shows that it is possible to detect this foveal polarization signature without the requirement that the spot of laser light be scanned or moved around the fovea. The no-moving-parts, birefringence-based fixation monitor produced a signal ND that peaked during central fixation (Fig. 8), indicating that this approach can be utilized to detect foveal fixation. With the present apparatus, $\mathrm{ND} > 0.15$, after background correction, appears to be a good threshold for central fixation. In addition, this method does not need eye-gaze calibration, which is a significant advantage over most other instruments used to monitor or track the direction of gaze.

The computer modeling involving the BPEI data showed that corneal birefringence can adversely influence the precision of this device by changing the orientation of the bow tie. Although with the majority of eyes the orientation is close enough to 45 deg to guarantee values above the threshold for central fixation, there are a small number of subjects where the rotation of the bow tie would be too much for accurate fixation detection. The suggested fixed corneal compensator

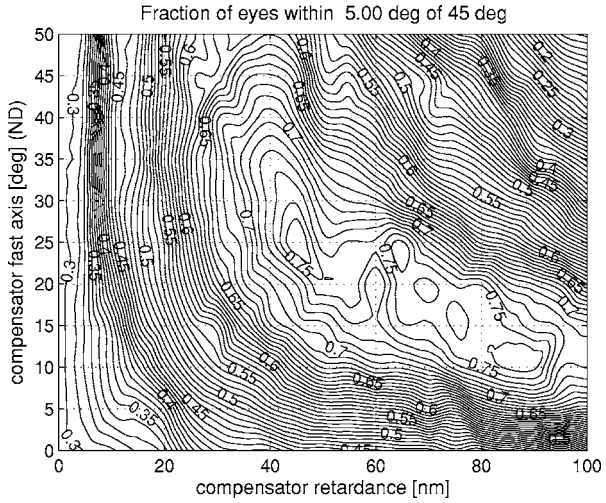

Fig. 11 Calculating an optimal fixed corneal compensator: fraction of eyes (RE+LE) falling within ±5 deg of 45 deg bow-tie orientation, as a function of compensator retardance and fast axis azimuth.

would improve the precision significantly. A large amount of abnormal ocular torsion, enough to give an abnormal azimuth to the corneal birefringence, could decrease the signal quality, but abnormal ocular torsion of more than 10 deg is quite rare. The effect of head tilts would produce similar artifacts. However, errors from head tilts are to a certain extent avoidable by either tilting the apparatus to be aligned with the head tilt, or orienting the head to be aligned with the apparatus.

The main difficulty with this device appears to be the low signal-to-noise ratio (SNR) of roughly 0.07 to 0.14 due to light reflected from the sclera, cornea, and face. The time-synchronous averaging greatly improved the stability of the parameters measured and the reliability of the fixation and gaze-position measures calculated. But it should also be noted that an unexpected change of background of several percent (i.e., due to a slight movement of the face after the last background measurement) would be incorporated into the eventual signal and would adversely influence measurement accuracy. A "Zorro" mask made of black felt decreased the background signal from facial reflections about three-fold and greatly improved measurement stability in ND-based central fixation applications. Unfortunately, such a mask cannot be used in a clinical pediatric application, which is the primary target application for our device. Another approach to reduce the effect of the reflections from the sclera, cornea, and face would be to modify the system such that the four light spots are fired sequentially, rather than simultaneously, i.e., by using four laser diodes. This would decrease background interference roughly four-fold, because reflections from the face back into the system would be reduced essentially four-fold.

The SNR can be improved by optimizing the modulation frequency, the duration of the epoch for signal averaging, and the number of waveforms being averaged. Signal processing methods such as matched filtering can help select only the good wave shapes for background, and for background plus fundus, and discard the wave shapes distorted by unwanted motion. Increasing laser power within the safety limits would further improve SNR, because the fundus would preserve polarization to a much higher extent than facial skin.

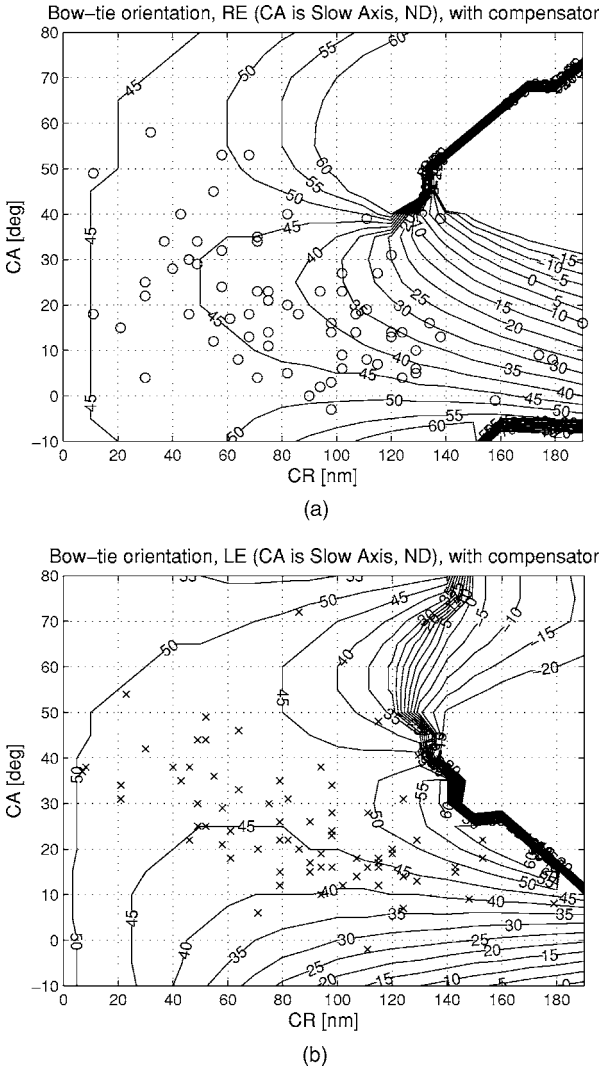

Fig. 12 Expected bow-tie orientation as a function of corneal retardance and corneal azimuth, with an optimal fixed corneal compensator. The BPEI data were blended in. Please compare to Fig. 9. (a) Right eye (71 eyes) and (b) left eye (72 eyes).

Possible media opacities, such as corneal scars or partial cataracts, and likewise small pupils, are likely to influence device performance negatively by lowering the value of ND at central fixation. Therefore, a lower threshold could be considered when using the device with such subjects.

5 Conclusion

We present a no-moving-parts fixation monitor that utilizes four spots of linearly polarized light impinging on different parts of the bow-tie pattern of polarization states reflected from the fovea. The light reflected from the fundus is imaged through a quarter-wave plate and a polarizer onto a four-quadrant photodetector. At central fixation, two of the light spots are aligned with the bright arms, and two are aligned with the dark arms of the bow-tie pattern. The four signals from the quadrant photodetector are combined in a simple linear combination ND, which reaches its maximum at central fixation. The device does not need calibration for each sub-

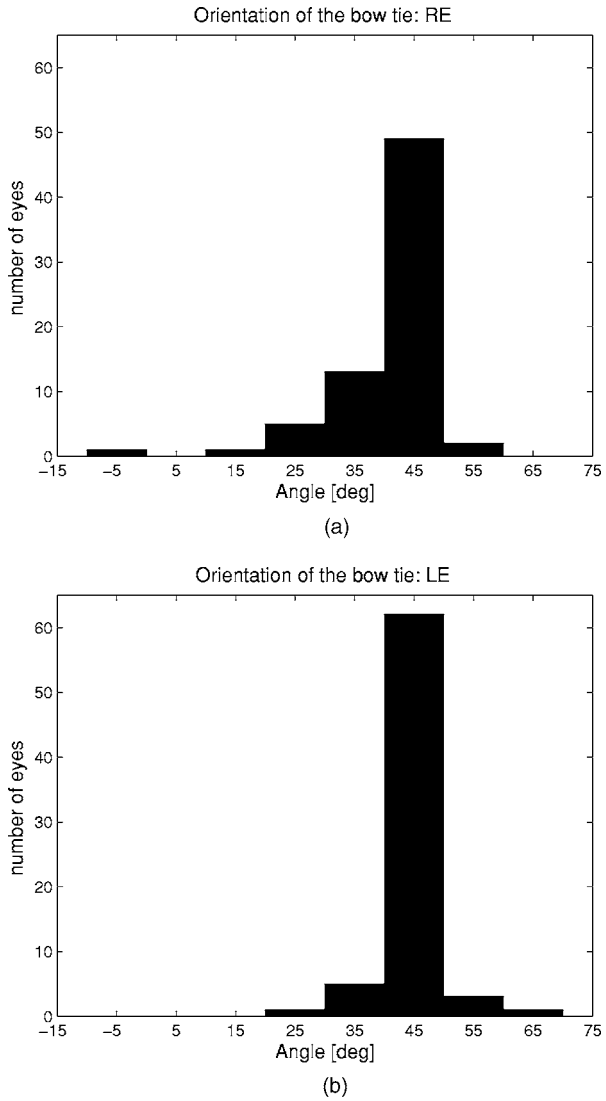

Fig. 13 Distribution of the bow-tie orientation angle from Fig. 12 (BPEI data with an optimal fixed corneal compensator). Please compare to Fig. 10. (a) Right eye (71 eyes) and (b) left eye (72 eyes).

ject. Our computer simulation and preliminary tests on human eyes demonstrate the feasibility of this type of fixation monitor. An improved signal-to-noise ratio in the signals obtained will be necessary for a robust instrument.

Acknowledgments

1. This work was supported by awards from Research to Prevent Blindness and the Alcon Research Institute, by National Institutes of Health (NIH) grant EY12883, and by gifts from Herbert Liebich, Janet and Dewey Gargiulo, and Helen and Robert Leighton. 2. The authors thank Robert W. Knighton and XiangRun Huang from the McNight Vision Research Center, Bascom Palmer Eye Institute, University of Miami School of Medicine, for the corneal birefringence data from 73 human subjects. 3. Carl Zeiss Meditec provided assistance with the GDx-VCC manuals and latest software update. 4. David Kays from the Wilmer Eye Institute provided technical assistance.

References

1. H. B. klein Brink and G. J. van Blokland, "Birefringence of the human foveal area assessed in vivo with Mueller-matrix ellipsometry," *J. Opt. Soc. Am. A* **5**(1), 49–57 (1988).
2. A. W. Dreher, K. Reiter, and R. N. Weinreb, "Spatially resolved birefringence of the retinal nerve fiber layer assessed with a retinal laser ellipsometer," *Appl. Opt.* **31**, 3730–3735 (1992).
3. D. L. Guyton, D. G. Hunter, S. N. Patel, J. C. Sandruck, and R. L. Fry, "Eye fixation monitor and tracker," U.S. Patent No. 6,027,216 (Feb. 22, 2000).
4. D. G. Hunter, S. N. Patel, and D. L. Guyton, "Automated detection of foveal fixation by use of retinal birefringence scanning," *Appl. Opt.* **38**(7), 1273–1279 (1999).
5. D. G. Hunter, J. C. Sandruck, S. Sau, S. N. Patel, and D. L. Guyton, "Mathematical modeling of retinal birefringence scanning," *J. Opt. Soc. Am. A* **16**(9), 2103–2111 (1999).
6. S. Duke-Elder, N. Ashton, R. J. H. Smith, and M. Lederman, "Entoptic observations," Chap. 15 in *The Foundations of Ophthalmology, System of Ophthalmology VII*, pp. 457, C. V. Mosby Company, St. Louis, MO (1968).
7. D. Nassif, B. Gramatikov, D. Guyton, and D. Hunter, "Pediatric vision screening using binocular retinal birefringence scanning," *Proc. SPIE* **4951**, 9–20 (2003).
8. N. Lopez-Gil and P. Artal, "Comparison of double-pass estimates of the retinal-image quality obtained with green and near-infrared light," *J. Opt. Soc. Am. A* **14**(5), 961–971 (1997).
9. N. P. Zagers, J. van de Kraats, T. T. Berendschot, and D. van Norren, "Simultaneous measurement of foveal spectral reflectance and cone-photoreceptor directionality," *Appl. Opt.* **41**(22), 4686–4696 (2002).
10. A. E. Elsner, S. A. Burns, J. J. Weiter, and F. C. Delori, "Infrared imaging of sub-retinal structures in the human ocular fundus," *Vision Res.* **36**(1), 191–205 (1996).
11. D. Sliney and M. Wolbarsht, *Safety with Lasers and Other Optical Sources*, Plenum Press, New York (1980).
12. W. A. Shurcliff, *Polarized Light: Production and Use*, Harvard University Press, Cambridge, MA (1962).
13. D. S. Klieger, J. W. Lewis, and C. E. Randall, *Polarized Light in Optics and Spectroscopy*, Academic Press, San Diego, CA (1990).
14. S. Duke-Elder, *The Anatomy of the Visual System, System of Ophthalmology*, pp. 266–269, C.V. Mosby Co., St. Louis, MO (1961).
15. S. N. Patel, "Analysis of foveal birefringence to monitor eye fixation." Master's Thesis, Johns Hopkins Univ., Baltimore, MD (1995).
16. R. W. Knighton and X. R. Huang, Linear birefringence of the central human cornea, *Invest. Ophthalmol. Visual Sci.* **43**(1), 82–86 (2002).
17. R. N. Weinreb, C. Bowd, D. S. Greenfield, and L. M. Zangwill, "Measurement of the magnitude and axis of corneal polarization with scanning laser polarimetry," *Arch. Ophthalmol. (Chicago)* **120**(7), 901–906 (2002).
18. Q. Zhou and R. N. Weinreb, "Individualized compensation of anterior segment birefringence during scanning laser polarimetry," *Invest. Ophthalmol. Visual Sci.* **43**(7), 2221–2228 (2002).